Correlated Dynamics in a Synthetic Lattice of Momentum States

Fangzhao Alex An, Eric J. Meier, Jackson Ang'ong'a, and Bryce Gadway

Correlated dynamics in a synthetic lattice of momentum states

Fangzhao Alex An,[*] Eric J. Meier,[*] Jackson Ang'ong'a, and Bryce Gadway[†]

Department of Physics, University of Illinois at Urbana-Champaign, Urbana, IL 61801-3080, USA

(Dated: December 19, 2017)

We study the influence of atomic interactions on quantum simulations in momentum-space lattices (MSLs), where driven transitions between discrete momentum states mimic transport between sites of a synthetic lattice. Low energy atomic collisions, which are short ranged in real space, relate to nearly infinite-ranged interactions in momentum space. However, the added exchange energy between atoms in distinguishable momentum states leads to an effectively attractive, finite-ranged interaction between atoms in momentum space. In this work, we observe the onset of self-trapping driven by such interactions in a momentum-space double well, paving the way for more complex many-body studies in tailored MSLs. We consider the types of phenomena that may result from these interactions, including the formation of chiral solitons in zigzag flux lattices.

Quantum simulation with ultracold atoms [1, 2] has been a powerful tool in the study of many-body physics and nonequilibrium dynamics. There has been recent interest in extending quantum simulations from real-space potentials to synthetic lattice systems composed of discrete internal [3, 4] or external [5] states. These synthetic dimensions enable many unique capabilities for quantum simulation, including the ability to engineer nontrivial topology [4, 6] and higher dimensions [3].

Our recent development of momentum-space lattices (MSLs), based on the use of discrete momentum states as effective sites, has introduced a fully synthetic approach to simulating lattice dynamics [7–11]. As compared to partially synthetic approaches [12, 13], fully synthetic lattices offer the possibility of studying coherent internal-state dynamics that are decoupled from any motional entropy [14]. Moreover, synthetic lattices offer a microscopic control over all system parameters, analogous to that found in photonic simulators [15, 16] but with a more natural path to exploring the influence of interactions.

MSLs provide a bottom-up approach to engineering designer Hamiltonians with field-driven transitions. Considering non-interacting atoms initially at rest and driven by a single pair of counter-propagating lasers with wavelength λ and wavevector $k = 2\pi/\lambda$, a discrete set of momentum states $p_n = 2n\hbar k$ may be coupled, having energies $E_p^0 = p_n^2/2m = 4n^2 E_R$, for integer state index n, atomic mass m, and photon recoil energy $E_R = \hbar^2 k^2/2m$. Individual addressing of the unique Bragg transitions allows us to engineer, with full local and temporal parameter control, the single-particle tight-binding model

$$H^{\text{sp}} \approx -\sum_{n,\alpha} t_{n,\alpha}(e^{i\varphi_{n,\alpha}}\hat{c}_{n+\alpha}^\dagger \hat{c}_n + \text{h.c.}) + \sum_n \varepsilon_n \hat{c}_n^\dagger \hat{c}_n \ , \ (1)$$

where $\hat{c}_n$ ($\hat{c}_n^\dagger$) is the annihilation (creation) operator for the state with momentum p_n. Here, tunneling of order α (e.g. $\alpha = 1$ and 2 for nearest- and next-nearest-neighbor tunnelings, respectively) is controlled through the amplitudes and phases of individual frequency components used to drive Bragg transitions of order α [17]. Similarly, an effective potential landscape of site energies ε_n

is controlled by small detunings from Bragg resonance. A detailed description of the mapping of our system onto this Hamiltonian can be found in Refs. [7, 8].

While MSLs have seen success in engineering diverse single-particle Hamiltonians [8–11], the prospects for studying interactions and correlated dynamics have not yet been examined. In real-space atomic systems, correlated physics has largely been driven by two-body contact interactions [18, 19], which are nearly infinite ranged in momentum space (i.e. with an energy independent of relative momentum for two colliding, distinguishable atoms). In one dimension, where collisions are mode-preserving, the resulting all-to-all interactions in MSLs would appear incapable of driving correlated behavior.

This description is incomplete, however, as the quantum statistics of identical bosonic atoms in MSLs create a structured interaction profile in momentum space. For just two identical bosons, the symmetrization of the two-body wave function adds an exchange interaction (in addition to the direct term) when the two particles collide in distinguishable motional states [20–23]. For positive scattering lengths, this additional long-range repulsion between atoms in distinct momentum states can alternatively be viewed as an effective attraction between atoms occupying the same momentum state. This combination of momentum-independent collisions and quantum statistics results in several hallmark features of bosonic quantum fluids: the Bogoliubov quasiparticle dispersion, distinct transport properties of heat and sound [24], and enhanced condensation in weakly repulsive gases [25].

MSL experiments typically do not probe isolated pairs of colliding atoms, so we should consider interactions of atoms in macroscopically populated momentum orders. Most experiments begin with all population in a condensate at rest with applied couplings to nonzero momentum states, and in this limiting case of initial, weak excitations, the role of interactions maps onto the well-studied scenario of Bogoliubov excitations [20, 32, 33]. We briefly consider this experimentally relevant, albeit restricted, scenario as a simple description of how superfluid screening can influence the distinguishability of
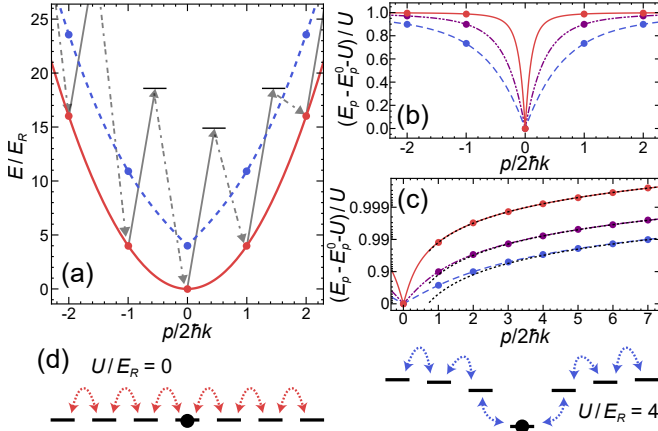
FIG. 1. **Interaction shifts of Bragg tunneling resonances.** **(a)** Energy dispersion of non-interacting massive atoms E_p^0 (red solid line) and Bogoliubov dispersion E_p of a homogeneous gas with weak repulsive interactions and a mean-field energy $U = 4E_R$ (blue dashed line), for recoil energy E_R. Gray lines denote laser fields used to couple adjacent momentum states. **(b)** Effective momentum-space lattice site energies (with a common shift of U removed and renormalized to U) experienced by weakly-coupled excitations of a macroscopically populated $p = 0$ condensate, shown for $U/E_R = 0.1$, 1, and 4 (solid red, dash-dotted purple, and dashed blue lines, respectively). **(c)** Curves as in (b), but plotted on a semi-log scale for a larger range of momenta, compared to the form $U - U^2/2E_p^0$ (dotted black lines) relevant in the free-particle limit ($E_p^0 \gg 2U$). **(d)** Depiction of site energies shifted by interactions with a $p = 0$ condensate for $U/E_R = 0$ and $U/E_R = 4$.

momentum states, and thus the range of the effective attractive interaction. The general description of the range of interactions for many macroscopically populated momentum states is highly nontrivial, but when the total density or total interaction strength is sufficiently low such that the effects of screening are negligible, then an effectively site-local attraction is recovered.

Considering the Bogoliubov spectrum, we assume a uniform number density ρ_N relating to a homogeneous mean-field energy $U = g\rho_N$, for interaction parameter $g = 4\pi\hbar^2 a/m$ and s-wave scattering length a. While repulsive interactions raise the energy of $p = 0$ condensate atoms by U, high-momentum excitations ($E_p^0 \gg 2U$) experience an interaction energy shift of roughly $2U$ due to both direct and exchange interactions with the $p = 0$ condensate. For a general momentum p, the Bogoliubov quasiparticle excitations have an energy $E_p = U + \sqrt{E_p^0(E_p^0 + 2U)}$. Figure 1 depicts this modified energy dispersion, along with the form of the effective interaction-dependent shifts to the MSL site energies, which relate to the difference in energy between the final state and the initial $p = 0$ state. The interaction has an effective range in momentum space which increases for increasing U (Figs. 1(b,c)), reflecting the in-

fluence of screening on the distinguishability of the states with nonzero momentum. In the limit of low interaction strengths ($2U \ll 4E_R$), these states become fully distinguishable and the interaction is effectively site local. We note that in principle, the interactions with the zero-momentum superfluid are expected to vanish for excitations with extremely large momenta ($p \gg \hbar/a$) due to energy-dependent corrections to the scattering, but such extreme conditions are beyond current experiments.

In our system of Bose-condensed ^{87}Rb atoms [8], we can directly probe the interaction energy shifts of the momentum states through Bragg spectroscopy [20, 32, 33]. For our laser wavelength of 1064 nm, first-order Bragg resonances are expected at frequency detunings of $\pm 4E_R/\hbar \approx \pm 2\pi \times 8.1$ kHz for non-interacting atoms. As displayed in Figs. 2(a,b), we measure an average shift of these first-order Bragg resonances by $2\pi \times 1.14(5)$ kHz. The shifts to the ± 1 transitions are slightly different due to nonzero initial momentum of the condensate, and we have shifted the Bogoliubov dispersion in Fig. 2(b) to account for this.

As a first experimental study, we explore the influence of momentum-space interactions on population dynamics in a coupled double well. We initialize all of the population in the left well ($p = 0$ state), with a large initial energy bias Δ_i inhibiting tunneling between the wells. This bias $|\Delta_i|/\hbar = 2\pi \times 8$ kHz is chosen to greatly exceed the tunneling energy $t/\hbar \approx 2\pi \times 390$ Hz. As depicted in Fig. 2(c), the bias is linearly swept through zero (single particle resonance) to a final value $\Delta_f = -\Delta_i$ over 1 ms, similar to the methods of Ref. [34]. We consider both a positive sweep ($\Delta_i < 0$ to $\Delta_f > 0$) and a negative sweep (vice versa).

In the absence of interactions, the dashed curves in Fig. 2(d) show that the amount of population transferred is roughly independent of the sweep direction, with a slight difference stemming from initial condensate momentum of $-0.018\hbar k$. [26]. In contrast, the presence of site-dependent, attractive interactions causes a highly asymmetric, direction-dependent response in the population dynamics. Comparing the positive sweep data to the single particle theory, we find that population begins to transfer earlier and more population is transferred at the ramp's end. For the negative sweep data, interactions cause self-trapping, leading to slightly lower, delayed population transfer.

To perform simulations, we consider a simplified description of the exact interacting system, which in general is highly non-trivial and depends on the total density and exact distribution of all site populations. First, we assume that all momentum states occupy the same spatial mode, ignoring effects of spatial separation. Next, we assume that the allowed momenta relate to fully distinguishable quantum states. Thus the momentum-space interaction becomes completely site-local, an assumption which is only approximately true for our experimental
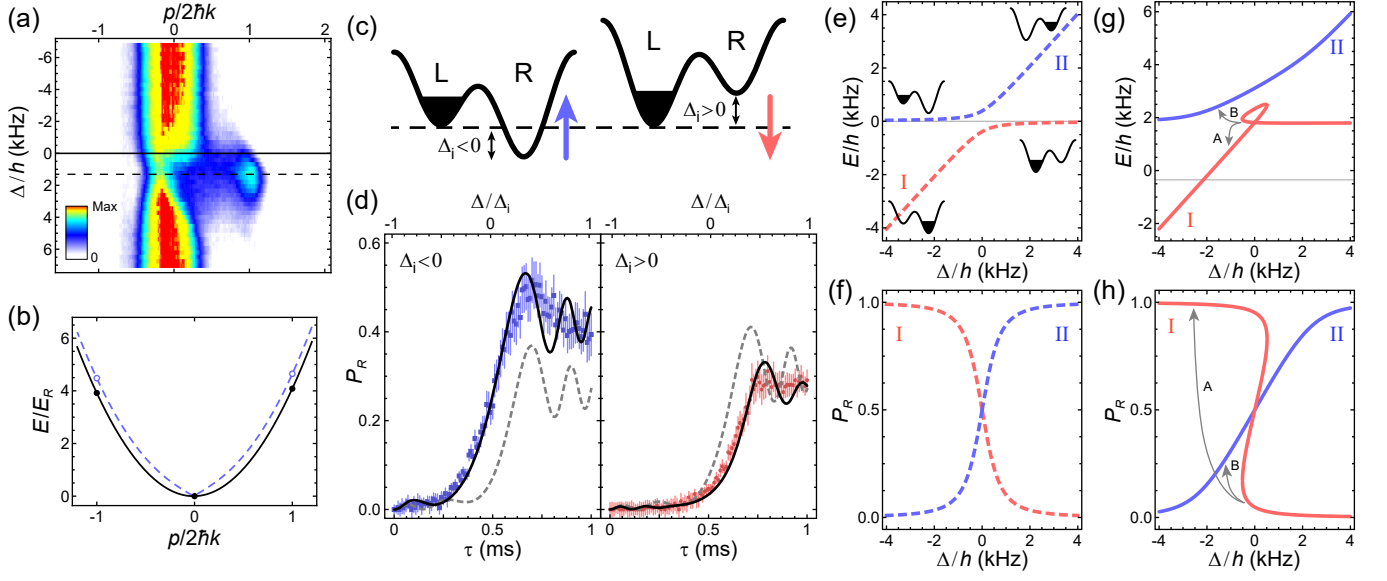
FIG. 2. **Interaction effects in a momentum-space double well.** (a) Bragg spectroscopy of the $0 \rightarrow 1$ transition showing an interaction-driven shift (dashed line) of 1.31(3) kHz from single particle resonance (solid line). The momentum distributions, relating to the integrated optical density after 18 ms time of flight, show population transferred to the state $p = 2\hbar k$ by a 400 μs-long Bragg pulse vs. detuning from single-particle resonance Δ. (b) Measured shifts for both $0 \rightarrow \pm 1$ transitions overlaid onto the Bogoliubov dispersion (dashed blue, shifted by initial condensate momentum $-0.018\hbar k$) with single-particle dispersion for comparison (solid black). (c) Experimental protocol for double well sweeps. Population begins in left well (L) and transfers to the right well (R) as the imbalance Δ (detuning from single-particle resonance) is swept linearly across 0 (dashed line) in the positive (left, blue arrow) and negative (right, red arrow) directions over 1 ms. (d) Population in the right well P_R plotted vs. time τ (lower horizontal axis) and vs. the ratio of the bias to the initial bias Δ/Δ_i (upper horizontal axis). Positive (left, blue squares) and negative (right, red dots) sweeps are shown with single-particle predictions (dashed gray curves) and predictions taking into account the inhomogeneous density distribution with an average mean-field energy $U/\hbar \approx 2\pi \times 1.81$ kHz [26] (solid black curves). (e) Adiabatic energy levels (I and II) of the non-interacting double well vs. Δ. Cartoon insets depict the population distributions for large $|\Delta/\hbar|$. (f) Population projection of the adiabatic levels in (e) onto the right well vs. Δ. (g,h) Energy levels and population projections as in (e,f), but with an added homogeneous mean-field energy of $U/\hbar \approx 2\pi \times 1.81$ kHz. Gray arrows A and B on the negative sweep denote forced tunneling pathways as the population transfer overshoots due to self-trapping. Error bars in (b) and (d) denote one standard error of the mean.

conditions. Lastly, given that the number of atoms in experiment vastly exceeds the number of sites, we ignore quantum fluctuations and simply represent the condensate wave function by appropriately normalized complex amplitudes ϕ_n for the various discrete momentum states [35]. Additionally, to capture the inhomogeneous density distribution caused by the harmonic trap [32], we use a local density approximation, taking a weighted average of simulation curves with different homogeneous mean-field energies U ranging from 0 to a peak mean-field energy U_0 [26].

Under these conditions, the influence of momentum-space interactions may be captured by the nonlinear Schrödinger equation

$$ i\hbar\dot{\phi}_n = \sum_m H^{sp}_{mn}\phi_m + U[2 - |\phi_n|^2]\phi_n \ , \qquad (2) $$

where H^{sp}_{mn} is the matrix element of the single-particle Hamiltonian H^{sp} (Eq. (1)) associated with states p_m and p_n. The form of Eq. 2, which assumes the normalization condition $\sum_n |\phi_n|^2 = 1$, hints at the effectively at-

tractive, mode-local momentum-space interaction. We note that all interaction terms preserve the individual site populations, as mode mixing is disallowed for elastic, one-dimensional collisions and uniform density [35–37], except when considering multiple internal states [38] or a lattice-modified dispersion [39, 40].

The simulated dynamics for the double-well case, where $H^{sp} = \Delta(\tau) \ \hat{c}_1^\dagger \hat{c}_1 - t(\hat{c}_0^\dagger \hat{c}_1 + \hat{c}_1^\dagger \hat{c}_0)$ for time τ, are shown as solid curves in Fig. 2(d). These simulations reproduce the observed direction-dependent response, while the lack of oscillatory behavior in the data can be attributed to spatial decoherence between momentum orders. We performed a combined fit of the data from Figs. 2(a-d) to obtain values for tunneling energy $t/\hbar \approx 2\pi \times 390$ Hz, initial condensate momentum $-0.018\hbar k$, and a peak mean-field energy $U_0/\hbar \approx 2\pi \times 3.17$ kHz of our inhomogeneous density distribution, with an average mean-field energy of $U/\hbar \approx 2\pi \times 1.81$ kHz [26].

To better understand these direction-dependent results, we consider the adiabatic energy levels of this coupled two-level system [26] and their projections onto the

measured well populations. Without interactions, the Bragg-driven "tunneling" leads to an avoided crossing of the adiabatic energy levels (Fig. 2(e)), allowing for complete transfer between wells in the limit of an infinitely slow Δ sweep (Fig. 2(f)), independent of the sweep direction. In contrast, adding interactions introduces a swallow-tail-like loop structure with metastable branches (Fig. 2(g)) [41–43]. For a slow positive sweep (starting on the top branch), the avoided crossing is maintained, leading to full population transfer as seen in Fig. 2(h). For a slow negative sweep (starting on the lower branch), atoms are forced to tunnel between the energy branches (path B), relating to self-trapping in the initial left well as seen in Fig. 2(h). For finite sweep times as in our experiment, a combination of forced tunneling along pathways A and B leads to a transfer efficiency that depends on the sweep direction, but with less extreme of a distinction as compared an infinitely slow ramp.

We note that this type of swallow-tail structure is generic to systems with strong nonlinear interactions, relating to the breakdown of adiabaticity and the possibility of hysteretic response [42–45]. Such interactions may also allow the study of symmetry breaking [46] and two-mode entanglement [47] in momentum-space double wells. In particular, the generation of squeezed momentum states with the effectively mode-local interactions could lead to practical advances in inertial sensing [26]. Beyond double wells [34, 44, 46, 48–52], MSLs offer unique capabilities for engineering multiply-connected lattice geometries. Here we explore the influence of interactions on the particle dynamics in a zigzag lattice (Fig. 3), where artificial fluxes play a nontrivial role [53, 54].

We consider a zigzag lattice with uniform nearest and next-nearest neighbor tunneling $t_{n,1} = t_{n,2} \equiv t$ and a uniform magnetic flux φ (Fig. 3(a)). We initialize population to a single, central site ($n = 0$) and simulate dynamics following a tunneling quench. The normalized site populations P_n at various evolution times τ are shown in Fig. 3(b). For a positive flux value of $\pi/6$, dramatically different behavior is found for zero ($U/t = 0$), moderate ($U/t = 7.2$), and strong ($U/t = 12$) interactions. Without interactions, chiral currents are present, but with a rapid ballistic spreading of the atomic distribution. Moderate interactions stabilize the distribution, leading to soliton- or breather-like states [55]. For strong interactions, the atoms remain localized at $n = 0$ due to self-trapping.

To gain more insight into the general behavior for nonzero fluxes and varied interactions, we plot in Fig. 3(c) the average site position $\langle n \rangle$ and the population in the most-populated site $P_n^{\max}$ versus the interaction-to-tunneling energy ratio U/t, for a flux $\pi/6$ following a duration $\tau = 65\,\hbar/t$. For weaker interaction strengths $U/t \lesssim 5$, the initially localized wavepacket becomes highly delocalized (low $P_n^{\max}$), while on average the pop-
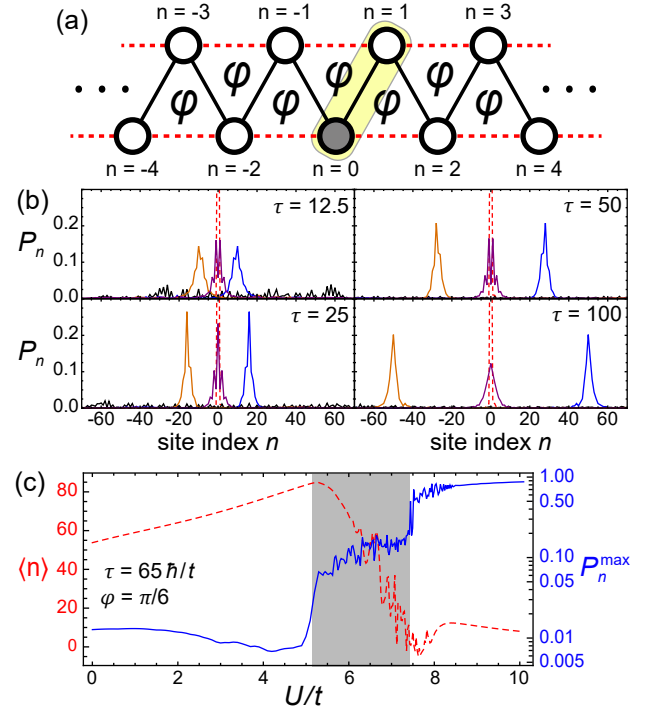
FIG. 3. **Interaction effects in a zigzag flux lattice.** (**a**) Cartoon depiction of atoms initialized at the central site ($n = 0$, gray) of a zigzag lattice with uniform magnetic flux φ. Nearest- (solid black) and next-nearest (dashed red) neighbor tunneling links have uniform amplitude t. Shaded yellow region indicates two-site unit cell. (**b**) Site population distributions for evolution times $\tau = \{12.5, 25, 50, 100\}\,\hbar/t$, shown for several combinations of interaction-to-tunneling ratios and flux values on a 401-site lattice: solid black denotes $(U/t, \varphi) = (0, \pi/6)$, rightmost solid blue for $(7.2, \pi/6)$, dashed red for $(12, \pi/6)$, solid purple for $(7.2, 0)$, and leftmost solid orange for $(7.2, -\pi/6)$. (**c**) Average site position $\langle n \rangle$ (red dashed line; left vertical axis with linear scale) and population in the most-populated site $P_n^{\max}$ (blue solid line; right vertical axis with logarithmic scale) versus U/t. Simulations are shown for $\varphi = \pi/6$ after an evolution time $\tau = 65\,\hbar/t$ on an 801-site lattice, with population never reaching the boundaries. Shaded gray region indicates chiral soliton stability.

ulation moves in a chiral fashion, reflecting an underlying spin-momentum locking of the flux lattice model [53]. In the intermediate regime ($5 \lesssim U/t \lesssim 7.5$), dynamics relating to chiral solitons can be found. The jump in the value of $P_n^{\max}$ to a finite, nearly fixed value relates to self-stabilization against wavepacket spreading. This self-stabilization can also be seen in Fig. 3(b), where the size of the chiral soliton wavepackets (blue and orange curves) remain nearly fixed, even as they propagate throughout the system. With increasing U/t, the solitons become more and more "massive" and travel less far (lower average site position $\langle n \rangle$) for the fixed evolution time ($65\,\hbar/t$). This eventually gives way to full self-trapping and the inhibition of chiral currents for $U/t \gtrsim 7.5$, with population localized to the initial site.

The chiral behavior observed for weak interactions stems from the presence of spin-momentum locking in the single-particle band structure, where an effective "spin" degree of freedom relates to the two sites of the zigzag lattice unit cell [53, 54] (shaded in Fig. 3(a)). The emergence of non-dispersing chiral solitons can be understood in terms of interaction-driven hybridization [56] of the two energy bands in the system. Stability is found as the interaction energy U starts to exceed the width of the lower energy band ($4t$), and complete self-trapping ensues when the interactions dominate over the combined band width ($6t$). The collective chiral behavior of the atoms under intermediate interactions is of fundamental interest to understanding how emergent behavior can arise from the interplay of interactions and synthetic gauge fields in kinetically frustrated systems [54, 57–60].

In addition to this novel behavior predicted to occur in momentum-space flux lattices [53], the ability to engineer arbitrary forms of disorder in MSLs should enable studies on the interplay of long-ranged momentum-space interactions and disorder-driven localization [61, 62]. Furthermore, while we have presently considered the influence of mode-preserving collisions (relevant to 1D, free-space elastic scattering) relating to effectively local nonlinearities in MSLs, other interesting types of correlated phenomena may result from mode-changing collisions [35–40], which would relate to correlated pair-hopping processes in MSLs.

---

* These authors contributed equally to this work
† bgadway@illinois.edu

[1] I. Bloch, J. Dalibard, and W. Zwerger, Rev. Mod. Phys. 80, 885 (2008).

[2] I. Bloch, J. Dalibard, and S. Nascimbène, Nat. Phys. 8, 267 (2012).

[3] O. Boada, A. Celi, J. I. Latorre, and M. Lewenstein, Phys. Rev. Lett. 108, 133001 (2012).

[4] A. Celi, P. Massignan, J. Ruseckas, N. Goldman, I. B. Spielman, G. Juzeliūnas, and M. Lewenstein, Phys. Rev. Lett. 112, 043001 (2014).

[5] H. M. Price, T. Ozawa, and N. Goldman, Phys. Rev. A 95, 023607 (2017).

[6] M. L. Wall, A. P. Koller, S. Li, X. Zhang, N. R. Cooper, J. Ye, and A. M. Rey, Phys. Rev. Lett. 116, 035301 (2016).

[7] B. Gadway, Phys. Rev. A 92, 043606 (2015).

[8] E. J. Meier, F. A. An, and B. Gadway, Phys. Rev. A 93, 051602 (2016).

[9] E. J. Meier, F. A. An, and B. Gadway, Nat. Commun. 7, 13986 (2016).

[10] F. A. An, E. J. Meier, and B. Gadway, Sci. Adv. 3, e1602685 (2017).

[11] F. A. An, E. J. Meier, and B. Gadway, Nat. Commun. 8, 325 (2017).

[12] M. Mancini, G. Pagano, G. Cappellini, L. Livi, M. Rider, J. Catani, C. Sias, P. Zoller, M. Inguscio, M. Dalmonte, and L. Fallani, Science 349, 1510 (2015).

[13] B. K. Stuhl, H.-I. Lu, L. M. Aycock, D. Genkina, and I. B. Spielman, Science 349, 1514 (2015).

[14] B. Yan, S. A. Moses, B. Gadway, J. P. Covey, K. R. A. Hazzard, A. M. Rey, D. S. Jin, and J. Ye, Nature 501, 521 (2013).

[15] A. Szameit and S. Nolte, J. Phys. B 43, 163001 (2010).

[16] A. Aspuru-Guzik and P. Walther, Nat. Phys. 8, 285 (2012).

[17] M. Kozuma, L. Deng, E. W. Hagley, J. Wen, R. Lutwak, K. Helmerson, S. L. Rolston, and W. D. Phillips, Phys. Rev. Lett. 82, 871 (1999).

[18] M. Greiner, O. Mandel, T. Esslinger, T. W. Hansch, and I. Bloch, Nature 415, 39 (2002).

[19] A. Mazurenko, C. S. Chiu, G. Ji, M. F. Parsons, M. Kanász-Nagy, R. Schmidt, F. Grusdt, E. Demler, D. Greif, and M. Greiner, Nature 545, 462 (2017).

[20] R. Ozeri, N. Katz, J. Steinhauer, and N. Davidson, Rev. Mod. Phys. 77, 187 (2005).

[21] M. Anderlini, P. J. Lee, B. L. Brown, J. Sebby-Strabley, W. D. Phillips, and J. V. Porto, Nature 448, 452 (2007).

[22] A. M. Kaufman, B. J. Lester, M. Foss-Feig, M. L. Wall, A. M. Rey, and C. A. Regal, Nature 527, 208 (2015).

[23] J. Larson, A. Collin, and J.-P. Martikainen, Phys. Rev. A 79, 033603 (2009).

[24] A. Griffin and E. Zaremba, Phys. Rev. A 56, 4839 (1997).

[25] R. P. Smith, R. L. D. Campbell, N. Tammuz, and Z. Hadzibabic, Phys. Rev. Lett. 106, 250403 (2011).

[26] See Supplemental Material for further discussion, details on the fitting procedures, adiabatic energy level calculations, further interpretation of double-well direction-dependent behavior, and prospects for momentum-space squeezing. The Supplemental Material includes Refs. [27–31].

[27] J. Estève, C. Gross, A. Weller, S. Giovanazzi, and M. K. Oberthaler, Nature 455, 1216 (2008).

[28] G.-B. Jo, Y. Shin, S. Will, T. A. Pasquini, M. Saba, W. Ketterle, D. E. Pritchard, M. Vengalattore, and M. Prentiss, Phys. Rev. Lett. 98, 030407 (2007).

[29] C. Gross, T. Zibold, E. Nicklas, J. Estève, and M. K. Oberthaler, Nature 464, 1165 (2010).

[30] W.-M. Zhang, D. H. Feng, and R. Gilmore, Rev. Mod. Phys. 62, 867 (1990).

[31] W. Muessel, H. Strobel, D. Linnemann, T. Zibold, J. Juliá-Díaz, and M. K. Oberthaler, Phys. Rev. A 92, 023603 (2015).

[32] J. Stenger, S. Inouye, A. P. Chikkatur, D. M. Stamper-Kurn, D. E. Pritchard, and W. Ketterle, Phys. Rev. Lett. 82, 4569 (1999).

[33] R. Lopes, C. Eigen, A. Barker, K. G. H. Viebahn, M. Robert-de Saint-Vincent, N. Navon, Z. Hadzibabic, and R. P. Smith, Phys. Rev. Lett. 118, 210401 (2017).

[34] Y.-A. Chen, S. D. Huber, S. Trotzky, I. Bloch, and E. Altman, Nature Physics 7, 61 (2010).

[35] M. Trippenbach, Y. B. Band, and P. S. Julienne, Phys. Rev. A 62, 023608 (2000).

[36] L. Deng, E. W. Hagley, J. Wen, M. Trippenbach, Y. Band, P. S. Julienne, J. E. Simsarian, K. Helmerson, S. L. Rolston, and W. D. Phillips, Nature 398, 218 (1999).

[37] S. L. Rolston and W. D. Phillips, Nature 416, 219 (2002).

[38] D. Pertot, B. Gadway, and D. Schneble, Phys. Rev. Lett. **104**, 200402 (2010).

[39] G. K. Campbell, J. Mun, M. Boyd, E. W. Streed, W. Ketterle, and D. E. Pritchard, Phys. Rev. Lett. **96**, 020406 (2006).

[40] N. Gemelke, E. Sarajlic, Y. Bidel, S. Hong, and S. Chu, Phys. Rev. Lett. **95**, 170404 (2005).

[41] S. Baharian and G. Baym, Phys. Rev. A **87**, 013619 (2013).

[42] L. Fallani, L. De Sarlo, J. E. Lye, M. Modugno, R. Saers, C. Fort, and M. Inguscio, Phys. Rev. Lett. **93**, 140406 (2004).

[43] S. B. Koller, E. A. Goldschmidt, R. C. Brown, R. Wyllie, R. M. Wilson, and J. V. Porto, Phys. Rev. A **94**, 063634 (2016).

[44] S. Eckel, J. G. Lee, F. Jendrzejewski, N. Murray, C. W. Clark, C. J. Lobb, W. D. Phillips, M. Edwards, and G. K. Campbell, Nature **506**, 200 (2014).

[45] C. Ryu, P. W. Blackburn, A. A. Blinova, and M. G. Boshier, Phys. Rev. Lett. **111**, 205301 (2013).

[46] A. Trenkwalder, G. Spagnolli, G. Semeghini, S. Coop, M. Landini, P. Castilho, L. Pezzè, G. Modugno, M. Inguscio, A. Smerzi, and M. Fattori, Nat. Phys. **12**, 826 (2016).

[47] S. Raghavan, H. Pu, P. Meystre, and N. Bigelow, Opt. Commun. **188**, 149 (2001).

[48] M. Albiez, R. Gati, J. Fölling, S. Hunsmann, M. Cristiani, and M. K. Oberthaler, Phys. Rev. Lett. **95**, 010402 (2005).

[49] S. Levy, E. Lahoud, I. Shomroni, and J. Steinhauer, Nature **449**, 579 (2007).

[50] L. J. LeBlanc, A. B. Bardon, J. McKeever, M. H. T. Extavour, D. Jervis, J. H. Thywissen, F. Piazza, and A. Smerzi, Phys. Rev. Lett. **106**, 025302 (2011).

[51] M.-S. Chang, Q. Qin, W. Zhang, L. You, and M. S. Chapman, Nat. Phys. **1**, 111 (2005).

[52] J. Tomkovič, W. Muessel, H. Strobel, S. Löck, P. Schlagheck, R. Ketzmerick, and M. K. Oberthaler, Phys. Rev. A **95**, 011602 (2017).

[53] F. A. An, E. J. Meier, and B. Gadway, (2017), arXiv:1705.09268.

[54] E. Anisimovas, M. Računas, C. Sträter, A. Eckardt, I. B. Spielman, and G. Juzeliūnas, Phys. Rev. A **94**, 063632 (2016).

[55] A. Trombettoni and A. Smerzi, Phys. Rev. Lett. **86**, 2353 (2001).

[56] M. E. Tai, A. Lukin, M. Rispoli, R. Schittko, T. Menke, D. Borgnia, P. M. Preiss, F. Grusdt, A. M. Kaufman, and M. Greiner, Nature **546**, 519 (2017).

[57] R. Khomeriki and S. Flach, Phys. Rev. Lett. **116**, 245301 (2016).

[58] F. Lin, C. Zhang, and V. W. Scarola, Phys. Rev. Lett. **112**, 110404 (2014).

[59] S. D. Huber and E. Altman, Phys. Rev. B **82**, 184502 (2010).

[60] D. Leykam, S. Flach, O. Bahat-Treidel, and A. S. Desyatnikov, Phys. Rev. B **88**, 224203 (2013).

[61] I. L. Aleiner, B. L. Altshuler, and G. V. Shlyapnikov, Nat. Phys. **6**, 900 (2010).

[62] B. Deissler, M. Zaccanti, G. Roati, C. D'Errico, M. Fattori, M. Modugno, G. Modugno, and M. Inguscio, Nat. Phys. **6**, 354 (2010).